# Effects of the microtubule nucleator Mto1 on chromosomal movement, DNA repair, and sister chromatid cohesion in fission yeast

Jacob Zhurinsky[a,†], Silvia Salas-Pino[a,b,†], Ana B. Iglesias-Romero[a,†], Antonio Torres-Mendez[a], Benjamin Knapp[b,c], Ignacio Flor-Parra[a,b], Jiyong Wang[d], Kehan Bao[d], Songtao Jia[d], Fred Chang[b,c,*], and Rafael R. Daga[a,b,*]

[a]Centro Andaluz de Biologia del Desarrollo, Universidad Pablo de Olavide, Seville 41013, Spain; [b]Department of Microbiology and Immunology, Columbia University College of Physicians and Surgeons, New York, NY 10032; [c]Department of Cell and Tissue Biology, University of California, San Francisco, San Francisco, CA 94143; [d]Department of Biological Science, Columbia University Medical Center, New York, NY 10027

**ABSTRACT** **Although the function of microtubules (MTs) in chromosomal segregation during mitosis is well characterized, much less is known about the role of MTs in chromosomal functions during interphase. In the fission yeast *Schizosaccharomyces pombe*, dynamic cytoplasmic MT bundles move chromosomes in an oscillatory manner during interphase via linkages through the nuclear envelope (NE) at the spindle pole body (SPB) and other sites. Mto1 is a cytoplasmic factor that mediates the nucleation and attachment of cytoplasmic MTs to the nucleus. Here, we test the function of these cytoplasmic MTs and Mto1 on DNA repair and recombination during interphase. We find that *mto1*Δ cells exhibit defects in DNA repair and homologous recombination (HR) and abnormal DNA repair factory dynamics. In these cells, sister chromatids are not properly paired, and binding of Rad21 cohesin subunit along chromosomal arms is reduced. Our findings suggest a model in which cytoplasmic MTs and Mto1 facilitate efficient DNA repair and HR by promoting dynamic chromosomal organization and cohesion in the nucleus.**

**Monitoring Editor**
Kerry S. Bloom
University of North Carolina

Received: May 30, 2019
Revised: Aug 27, 2019
Accepted: Aug 30, 2019

## INTRODUCTION

The dynamic organization of chromosomes within the eukaryotic nucleus is essential for the proper regulation of gene expression, ribosome synthesis, RNA processing and transport, and DNA replication and repair (Schneider and Grosschedl, 2007; Misteli and Soutoglou, 2009; Mekhail and Moazed, 2010; Matsuda *et al.*, 2017; Fabre and Zimmer, 2018). Chromosomal loci not only are located in certain positions within the nucleus, but they also exhibit characteristic movements in response to perturbations such as DNA damage (Dion *et al.*, 2012; Mine-Hattab and Rothstein, 2012). These movements may facilitate chromosomal processes such as DNA recombination and repair, but in general, functions of chromosomal movements remain to be fully elucidated. Movements may arise from chromosome-based forces and/or from cytoskeletal elements inside or outside the nuclear envelope (NE) (Harper *et al.*, 2004; Zhang *et al.*, 2006; Herbert *et al.*, 2008; Neumann *et al.*, 2012; Kim *et al.*, 2013; Uhler and Shivashankar, 2017). Factors at the NE and cytoskeletal elements play key roles in chromosomal organization. For instance, the Linker of Nucleoskeleton and Cytoskeleton (LINC) protein complexes in the NE have been implicated in linking microtubules (MTs) and actin in the cytoplasm to chromosomes at loci including centromeres and telomeres (Chikashige *et al.*, 2006; Crisp *et al.*, 2006; McGee *et al.*, 2006; Conrad *et al.*, 2008; Razafsky and Hodzic, 2009). One of the better characterized functions of the cytoskeleton and the LINC complexes is in nuclear positioning and movements (Malone *et al.*, 1999, 2003; Sjogren and Nasmyth, 2001; Daga *et al.*, 2006; Zhang *et al.*, 2007, 2009; Zhou *et al.*, 2009)

This article was published online ahead of print in MBoC in Press (http://www.molbiolcell.org/cgi/doi/10.1091/mbc.E19-05-0301) on September 4, 2019.

†These authors contributed equally to this work.

*Address correspondence to: Rafael R. Daga (rroddag@upo.es); Fred Chang (fred.chang@ucsf.edu).

Abbreviations used: ChIP, chromatin immunoprecipitation; Chr, chromosome; CPT, camptothecin; GFP, green fluorescent protein; HR, homologous recombination; LINC, Linker of Nucleoskeleton and Cytoskeleton; MBC, methyl benzimidazol-2-yl-carbamate; MMS, methyl-methane sulfonate; MTs, microtubules; NE, nuclear envelope; RFB, replication fork barrier; SPB, spindle pole body; YFP, yellow fluorescent protein.

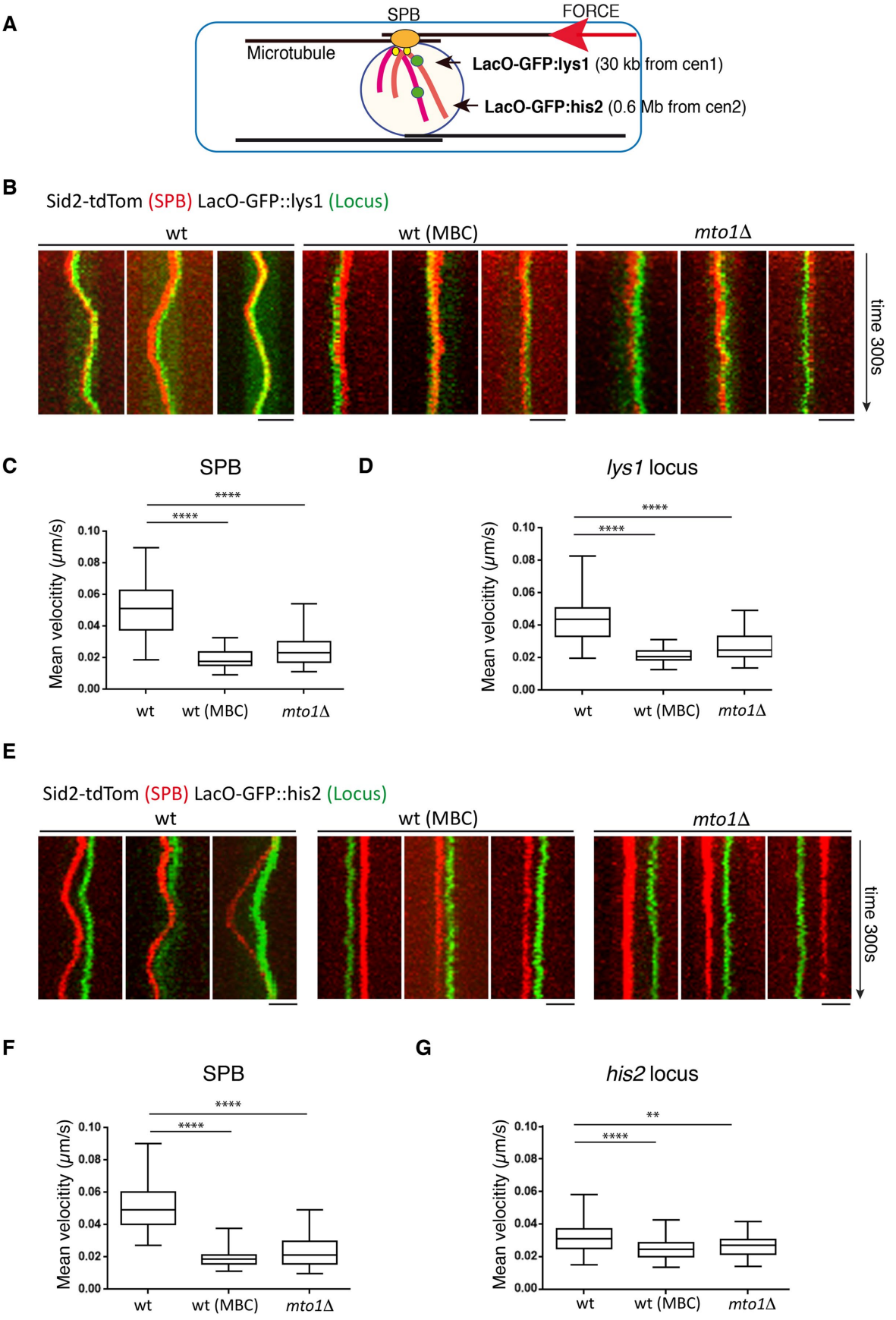


FIGURE 1: Microtubule-dependent movement of spindle pole bodies (SPBs) and DNA loci during interphase in *S. pombe*. (A) Schematic representation of interphase microtubule cytoskeleton in fission yeast, and its connections to the nucleus. The red arrow represents the direction of the force generated by MT polymerization after hitting the

Cytoskeleton-based forces may also affect the chromosomes inside the nucleus. There are well-documented cases showing cytoskeletal contributions to meiotic recombination. Meiotic chromosomal movements are driven by actin-based mechanisms in budding yeast (Conrad *et al.*, 2008; Koszul *et al.*, 2008; Christophorou *et al.*, 2015) and by MTs in the fission yeast (Ding *et al.*, 2004), *Caenorhabditis elegans* (Sato *et al.*, 2009), and *Drosophila* (Hampoelz *et al.*, 2011). In fission yeast, for instance, MTs drive dynein-dependent large oscillatory "horsetail" movements of the nucleus that are required for efficient meiotic homologous recombination (HR) (Ding *et al.*, 2004).

The role of interphase MTs in nonmeiotic cells in chromosomal behaviors is less clear. During interphase in fission yeast, MTs are organized into multiple cytoplasmic bundles attached at the spindle pole body (SPB) and other sites on the cytoplasmic face of the NE. No MTs are present inside the nucleus during interphase (Hoog and Antony, 2007). Cytoplasmic MTs exert pushing forces to produce oscillatory movements or rotations of the SPB and nucleus and dynamically position the nucleus at the cell middle (Tran *et al.*, 2001; Daga *et al.*, 2006). These MT forces are transmitted to the centromeres of all three chromosomes via SPB, which is located just outside the NE, through LINC complexes, Csi1, and other centromeric proteins (Hou *et al.*, 2012; Fernandez-Alvarez *et al.*, 2016). Although the connection between the SPB and centromere is bridged by kinetochore MTs during mitosis, this connection is MT independent during interphase. Centromeric loci and multiple noncentromeric loci have been demonstrated to exhibit MT-dependent movements, suggesting that these forces from cytoplasmic MTs mediate large-scale chromosomal movements inside the nucleus (Kim *et al.*, 2013).

The possible role of MTs in chromosomal organization and functions are not well understood. MTs, LINC complexes, and other NE factors have recently been implicated in DNA repair (Swartz *et al.*, 2014; Lottersberger *et al.*, 2015; Lawrence *et al.*, 2016). In *Schizosaccharomyces pombe*, LINC complexes composed of Sad1/Unc84 and Klarsicht/Anc1/SYNE1 homology protein Kms1 are recruited to sites of DNA damage (Swartz *et al.*, 2014); however, whether and how MTs themselves contribute to DNA repair has not been thoroughly explored.

Here, we test the role of cytoplasmic MTs on DNA repair in *S. pombe*. We use the *mto1*Δ mutant as a tool to specifically disrupt the association of cytoplasmic MTs with the NE. Mto1 is a MT nucleation factor that forms a complex with Mto2 and the γ-tubulin ring complex to promote MT nucleation at cytoplasmic sites (Sawin *et al.*, 2004; Venkatram *et al.*, 2004; Zimmerman and Chang, 2005; Samejima *et al.*, 2008; Bao *et al.*, 2018). *mto1*Δ cells exhibit a uniquely strong and specific cytoplasmic MT nucleation defect; they either lack cytoplasmic MTs completely or form a small number of MT bundles that are not physically connected to the nucleus. In these cells, consistent with the lack of MT attachment, the nucleus is abnormally shaped and/or mispositioned, and the SPB oscillations are not observed (Sawin *et al.*, 2004; Venkatram *et al.*, 2004; Zimmerman and Chang, 2005; Daga and Nurse, 2008). In contrast, during mitosis, MTs in *mto1*Δ mutants are nucleated normally inside the nucleus for spindle assembly. Consistent with a cytoplasmic function, Mto1 localizes to cytoplasmic MTOCs but has not been detected in the nucleus (Sawin *et al.*, 2004; Zimmerman and Chang, 2005). Here, we find that the inhibition of cytoplasmic MTs in the *mto1* mutant or by drug treatment leads to significant defects in DNA repair and HR. In investigating the cause of this phenotype, we unexpectedly find that these cells have defects in sister chromatid pairing and loading or maintenance of the cohesin Rad21. Thus, these findings provide new insights into the role of MTs and this MT nucleation factor in chromosomal organization and maintenance.

## RESULTS

### Interphase MTs are required for SPB and chromosomal movements

We tested the effect of cytoplasmic MTs and Mto1 on the movement of the SPB and chromosomes. We imaged live fission yeast cells in which the SPB was marked with Sid2-Tomato and two different chromosomal loci were marked with LacO arrays that were bound by green fluorescent protein (GFP)-LacI at *lys1* and *his2* loci, which are 30 kb away from centromere 1 and 0.6 Mb away from centromere 2, respectively (Figure 1A) (Molnar *et al.*, 2003). In wild-type cells, the SPB and the *lys1* locus moved together in oscillatory movements with approximately the same mean velocity (Figure 1, B–D). The *his2* locus also displayed oscillatory movements similar to the SPB (Figure 1E). This chromosomal locus usually moved in the same direction as the SPB, but with reduced mean velocity relative to the SPB (Figure 1, E–G). These movements are dependent on MTs, as they were abAolished after treatment with the MT-depolymerizing drug methyl benzimidazol-2-yl-carbamate (MBC) (Figure 1, B–G). Similarly, in the *mto1*Δ mutant, the oscillatory movements of the SPB and both chromosomal loci were absent (Figure 1, B–G). Thus, MTs and Mto1 are needed for large movements of chromosomes observed during interphase.

### *mto1*Δ and NE protein mutants are sensitive to DNA damage

We next tested whether MT-dependent movements contribute to DNA repair. As MBC inhibits mitotic cell cycle progression, we initially focused on characterizing the *mto1*Δ mutant, which has a more specific defect in interphase MTs (Sawin *et al.*, 2004; Venkatram *et al.*, 2004; Zimmerman and Chang, 2005). We used a standard spot growth assay to measure sensitivity to DNA-damaging agents. We found that *mto1*Δ cells are sensitive to methyl-methane sulfonate (MMS), camptothecin (CPT), and γ-irradiation (Figure 2, A and B) (see also Swartz *et al.*, 2014), which produce DNA damage that requires HR for its repair. They were not, however, sensitive to 254-nm UV irradiation and only mildly sensitive to hydroxyurea (Figure 2A), both of which cause different types of DNA damage.

cell tips. Black arrows indicate the position of the *lys1* and *his2* loci. ChrI/ChrII, chromosome I/II. The SPB is depicted in orange. Centromeres are depicted in yellow. (B) Kymographs showing movements of the SPB (marked with Sid2-tdTom) and chromosome at *lys1* locus in wild-type (wt) cells, wild-type cells treated with 10μg/ml MBC, and *mto1*Δ cells. Three representative cells are shown in each case. Kymographs were prepared from maximal projections of three *z*-sections with a step size of 0.4 μm. Time between frames is 2 s with total time of 300 s. Scale bar: 5 μm. (C, D) Graphs showing mean instantaneous velocities of the SPB and the *lys1* locus in the indicated strains and conditions ($n = 50$).
(E) Kymographs showing the SPB (marked with Sid2-tdTom) and chromosome at *his2* locus. Three representative cells are shown in each case. Kymographs were prepared from maximal projections of three *z*-sections with a step size of 0.4 μm. Time between frames is 2 s. Total time is 300 s. Scale bar: 5 μm. (F, G) Graphs showing mean instantaneous velocities of the SPB and *his2* locus ($n = 50$). **** denotes $p < 0.0001$ and ** denotes $p < 0.001$ from a Student's *t* test.

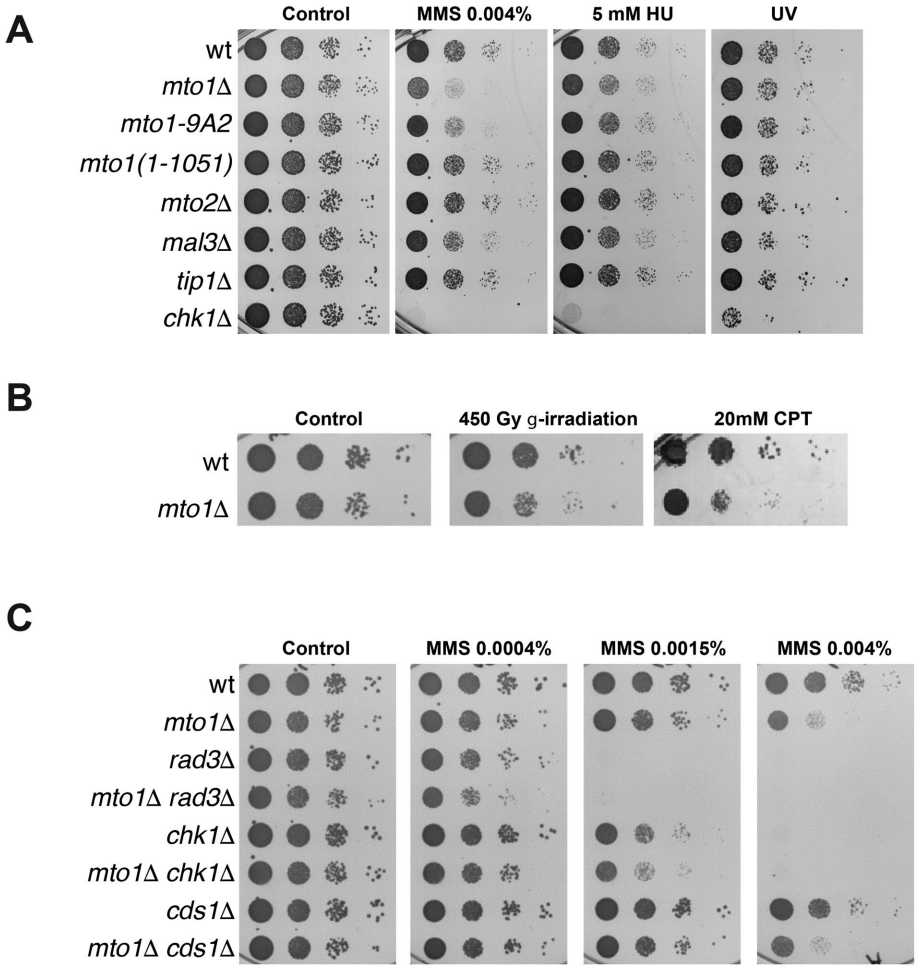


FIGURE 2: *mto1*Δ cells are sensitive to DNA damage. (A) Sensitivity of the indicated strains to a range of DNA-damaging agents. (B) Growth of wild-type and *mto1*Δ cells on agar plates was tested in the presence of 20 mM CPT and after irradiation with 450-Gy γ-rays. (C) Spot growth assays of the indicated strains in the presence of increasing concentrations of MMS. Cells were plated in YES plates at 30°C, and pictures were taken after 3–5 d (A–C).

This profile of DNA damage sensitivity suggests a defect of *mto1*Δ in HR-based DNA repair, or in the DNA damage checkpoint signaling.

We next tested what functions of Mto1 are needed for this phenotype by using different *mto1* alleles and also mutants affected in MT dynamics. The *mto1-9A2* mutant is defective in the interaction with the γ-tubulin complex and in MT nucleation and, as a consequence, shows reduced SPB movements (Samejima *et al.*, 2008). We found that this mutant was sensitive to MMS (Figure 2A). In contrast, the *mto1-1051* mutant, which is defective for MT attachment on the NE at non-SPB sites, but still exhibits MTs associated with the SPB and SPB movements (Samejima *et al.*, 2008), was not sensitive to MMS (Figure 2A). Other MT regulatory mutants, such as *mal3*Δ (EB1) and *tip1*Δ (CLIP170), which have effects on MT dynamics but retain some SPB movement, were not MMS sensitive (Figure 2A). Of note, the *mto2* mutant, which has a weak MT nucleation effect and still exhibits SPB movements (Samejima *et al.*, 2005; Venkatram *et al.*, 2005), was not MMS sensitive (Figure 2A). Thus, these results suggest that efficient DNA damage response is mediated by Mto1 functions in MT nucleation and SPB movements.

To evaluate the effect of chromosomal movements on the sensitivity to DNA damage, we tested *csi1*Δ and INM protein Lem2 or Ima1 mutants, which still display SPB movement but are defective in the link between the SPB or NE to chromosomes (Hiraoka *et al.*, 2011; Gonzalez *et al.*, 2012; Peters and Nishiyama, 2012; Steglich *et al.*, 2012; Barrales *et al.*, 2016). We found that *csi1*Δ, *lem2*Δ, and the double mutant *lem2*Δ *ima1*Δ were sensitive to MMS (Supplemental Figure S1A). These findings further support the role of chromatin–NE connections in the DNA damage response (Oza *et al.*, 2009; Ryu *et al.*, 2015; Xu, 2016)

Increased sensitivity to DNA damage could be due to defects in DNA repair or, alternatively, in DNA checkpoint signaling. To test this, we conducted epistasis tests of *mto1*Δ with *chk1*Δ, *cds1*Δ, and *rad3*Δ mutants that are defective in the DNA damage checkpoint, S-phase checkpoint, and general response to all types of DNA damage, respectively (Harrison and Haber, 2006). *mto1*Δ further increased MMS sensitivity of these checkpoint mutants (Figure 2C), suggesting that Mto1 does not merely act through these DNA checkpoint pathways. Cds1 regulates the response to S-phase DNA damage (Lindsay *et al.*, 1998; Rhind and Russell, 2000), and accordingly, *cds1*Δ cells were not sensitive to MMS (Figure 2C). Double *cds1*Δ *mto1*Δ mutants showed sensitivity to MMS that was similar to that of *mto1*Δ. Together, these results suggest that *mto1* mutants have a defect in HR-based DNA repair that is exacerbated in the absence of checkpoint signaling (*rad3*Δ, *chk1*Δ).

### Mto1 and microtubules affect DNA repair factories

To examine DNA repair in vivo, we imaged DNA repair factories marked with Rad52–yellow fluorescent protein (YFP) in live cells (Lisby *et al.*, 2003; Meister *et al.*, 2005). Wild-type cells typically form a small number of Rad52-YFP foci after S-phase during postreplication DNA repair. The disassembly of the repair factory is thought to occur upon repair (Meister *et al.*, 2003). In asynchronous cultures, 15% of wild-type cells contained a single Rad52-YFP focus (Figure 3, A and B) (Meister *et al.*, 2003, 2005). In *mto1*Δ cells, we found a twofold increase in the fraction of cells containing one Rad52 focus, and 10% of *mto1*Δ cells contained two foci (Figure 3, A and B). Time-lapse microscopy showed that, in wild-type cells, the lifetime of Rad52 factories is on average 60 min (Meister *et al.*, 2005) (Figure 3, C and D). In contrast, the repair factories in *mto1*Δ cells exhibited a twofold increase in Rad52-YFP intensity and an increase in average lifetime distribution (Figure 3, C–E). Mto1 therefore affects the dynamics of DNA repair factories.

To test whether MTs also affect Rad52 repair factory behavior, we determined the effects of depolymerizing cytoplasmic MTs in wild-type cells during a defined cell cycle period. For that, we imaged asynchronously growing cells in time lapse, introduced MBC (time 0), and then specifically tracked the individual cells in which MBC addition at $t_0$ coincided with late anaphase B (just before S-phase). As cells went through S and G2 phases in MBC, we observed the

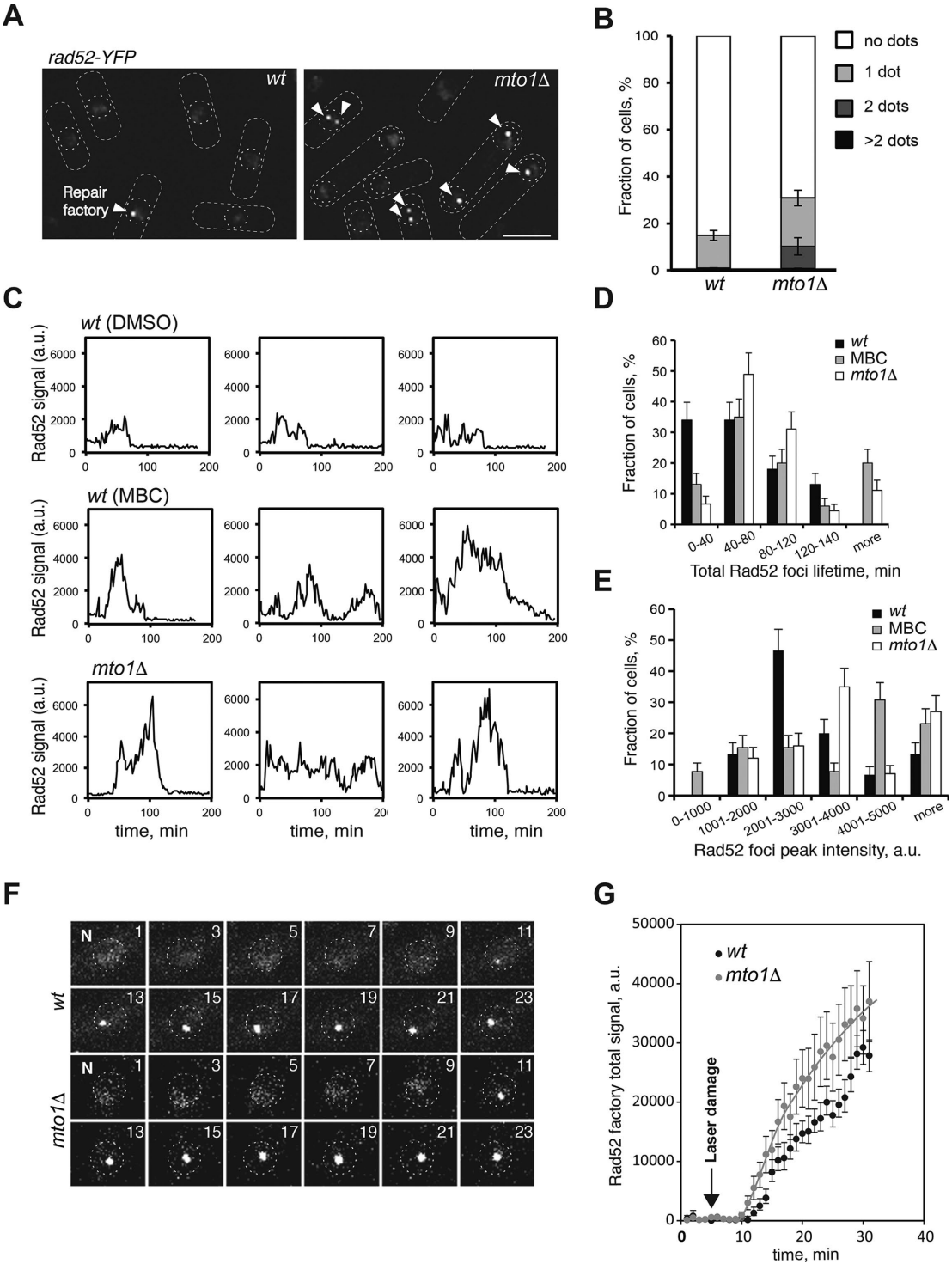


FIGURE 3: Mto1 and microtubules affect the dynamics of DNA repair factories. (A) Maximal-projection images of exponentially growing wild-type (wt) and *mto1*Δ cells expressing Rad52-YFP as marker of DNA repair factories (indicated by arrowheads). Scale bar: 5 µm. (B) Graphs showing the quantitation of factory number in wild-type and *mto1*Δ mutant ($n = 120$ cells). Error bars show SD of three independent experiments. (C) Time profiles of Rad52 factory intensity in wild-type cells, wild-type cells treated in late anaphase with 10 µg/ml MBC, and *mto1*Δ cells (three representative examples of each condition are shown). (D) Graphs showing total Rad52-YFP foci lifetime in the indicated strains and conditions. Error bars represent SD of three independent experiments. (E) Graph showing peak fluorescence intensity of Rad52-YFP foci in the indicated strains and conditions. There were 18 cells analyzed in D and E. Error bars represent SD. (F–G) Response to laser-induced DNA damage of wild-type and *mto1*Δ cells. Rad52-YFP was followed by time-lapse microscopy at 1-min time intervals. A single 10-ms pulse with a 355-nm laser was targeted at a fixed area of 500 nm of the nuclei of wild-type and *mto1*Δ cells at time 5 min. (F) Rad52-YFP repair factories after laser damage in a representative wild-type and *mto1*Δ cell. Time is indicated in minutes. N, nucleus. (G) Average intensity of Rad52-YFP repair factories is shown as a function of time ($n = 15$ cells for each strain). Error bars are SD.

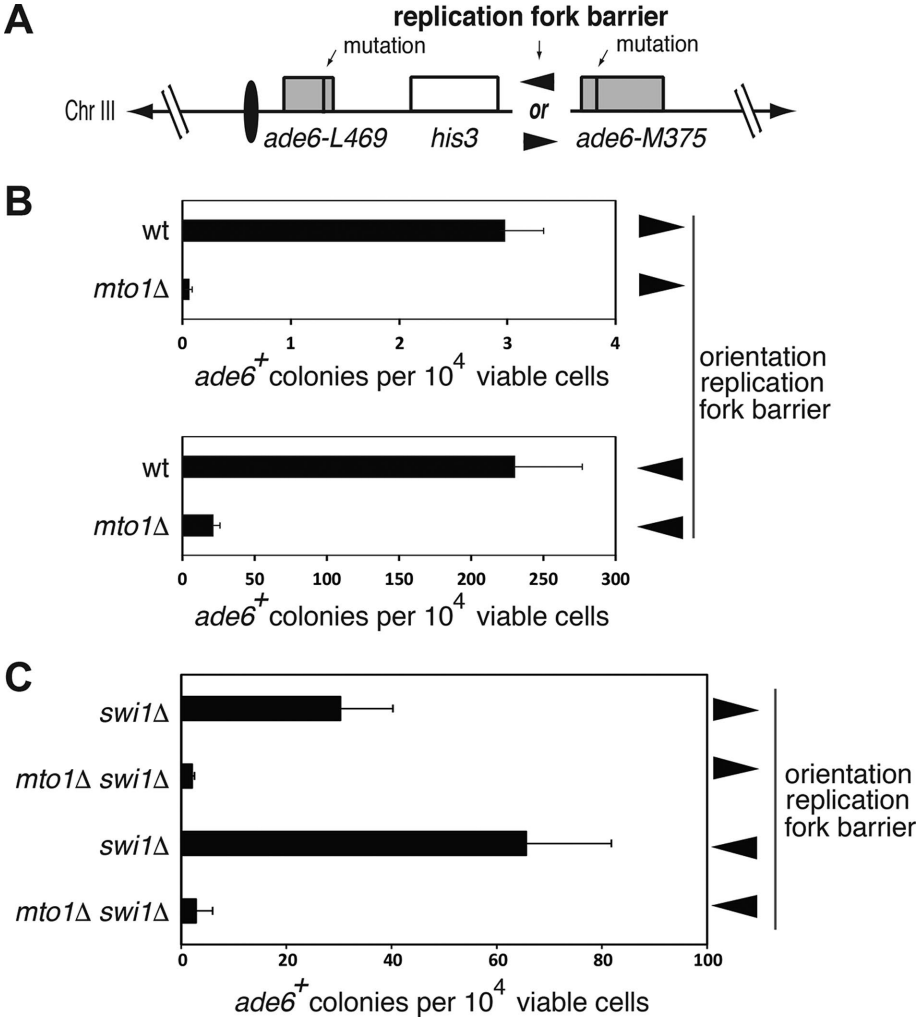


FIGURE 4: Efficiency of intrachromosomal homologous recombination is decreased in *mto1*Δ cells. (A) Schematic representation of the HR assay. Two variants containing a replication fork barrier (RFB) in the two opposite orientations are indicated by arrowheads. Centromere is depicted as a black oval. Notice the replication comes from an origin positioned on the right (toward the centromere). (B) Drop in the efficiency of HR in *mto1*Δ is seen in both recombination substrates that detect sister chromatid–based HR. Error bars represent SD of four independent experiments. wt, wild type. (C) Decreased recombination in *swi1*Δ *mto1*Δ genetic background. Error bars are SD of four independent experiments.

formation and resolution of the postreplicative repair factories marked by Rad52 foci. The intensities and lifetimes of the Rad52 foci were increased in MBC-treated cells relative to untreated cells, similar to what was seen in *mto1*Δ cells (Figure 3, C–E). Thus, inhibition of MTs after mitosis leads to abnormal DNA damage response in interphase.

To measure the dynamics of the DNA damage response in a quantitative manner, we induced DNA damage at a defined time point by applying a focused 410-nm laser beam on the nucleus of living cells. In both wild-type and *mto1*Δ cells, Rad52-YFP started to accumulate in a single dot at 5 min after irradiation, which steadily increased in intensity over the 30-min time course (Figure 3, F and G). Measurements of fluorescence intensity showed that Rad52-YFP intensity and the rate of accumulation were increased in *mto1*Δ compared with wild-type cells throughout the 30-min time course.

We examined whether Mto1 localizes to DNA repair factories and found that Mto1-mCherry was not detectable within the nucleus, as previously shown (Sawin *et al.*, 2004; Venkatram *et al.*, 2004; Zimmerman and Chang, 2005) (Supplemental Figure S2A). Specifically we could not detect Mto1 at DNA repair factories upon MMS-induced DNA damage (Supplemental Figure S2B).

Together, these experiments show that Mto1 and MTs affect the behavior of repair factories for postreplication repair and the repair of exogenous DNA damage, and they may do so indirectly from the cytoplasm.

### Homologous recombination is reduced in *mto1*Δ cells

As HR between sister chromatids is the primary pathway for DNA repair in G2 (Harrison and Haber, 2006), we assayed for possible defects in HR in the *mto1*Δ mutant. Intrachromosomal recombination (i.e., between sister chromatids) was assayed using a genetically based approach developed by Ahn *et al.* (2005). This assay uses strains containing the polar replication fork barrier (RFB) *RTS1* oriented either in the direction of the replication (toward the centromere) or in the opposite direction, between a direct repeat of ade6 heteroalleles located at the *ade6* locus on chromosome 3 (Chr III). This allowed us to measure HR induced by RFB, and much lower rates of spontaneous HR at this locus (Figure 4A). Recombination rates were decreased by 10-fold in *mto1*Δ strains in both recombination substrates (Figure 4B). The magnitude of the recombination defect is comparable to that seen in mutants in key recombination proteins such as Rhp51 (Ahn *et al.*, 2005). We also found a similar decrease of recombination efficiency in both replication fork substrates when *mto1* was deleted in the *swi1*Δ background (Ahn *et al.*, 2005), which abolished the difference between the two substrates (Figure 4C). In contrast, *mto1* had little effect on interchromosomal HR between the double strand break (DSB)-induced recombination of Chr III and an artificial homologous Chr III fragment (Prudden *et al.*, 2003) (Supplemental Figure S3, A and B). These findings indicate that Mto1 is required for efficient sister chromatid–based HR.

### Mto1 affects sister chromatid cohesion

Because DNA repair based upon HR during G2 requires proper pairing of sister chromatids (Birkenbihl and Subramani, 1992; Hartsuiker *et al.*, 2001; Jessberger, 2002), we next examined the effects of Mto1 and microtubules on sister chromatid cohesion. First, we imaged the dynamic behavior of GFP-labeled LacO arrays on chromosomal loci during the G2 phase in live cells. Time-lapse confocal imaging using GFP-labeled arrays at the *his2* locus revealed that sister chromatids during interphase exhibited occasional "breathing" events in which the labeled loci moved apart (>200 nm) to appear transiently as two dots and then came back together in a period of 2 s (Figure 5, A and B). This behavior was seen infrequently in wild-type cells, but this transient separation of the sister loci occurred more frequently in *mto1* mutant and cells treated with

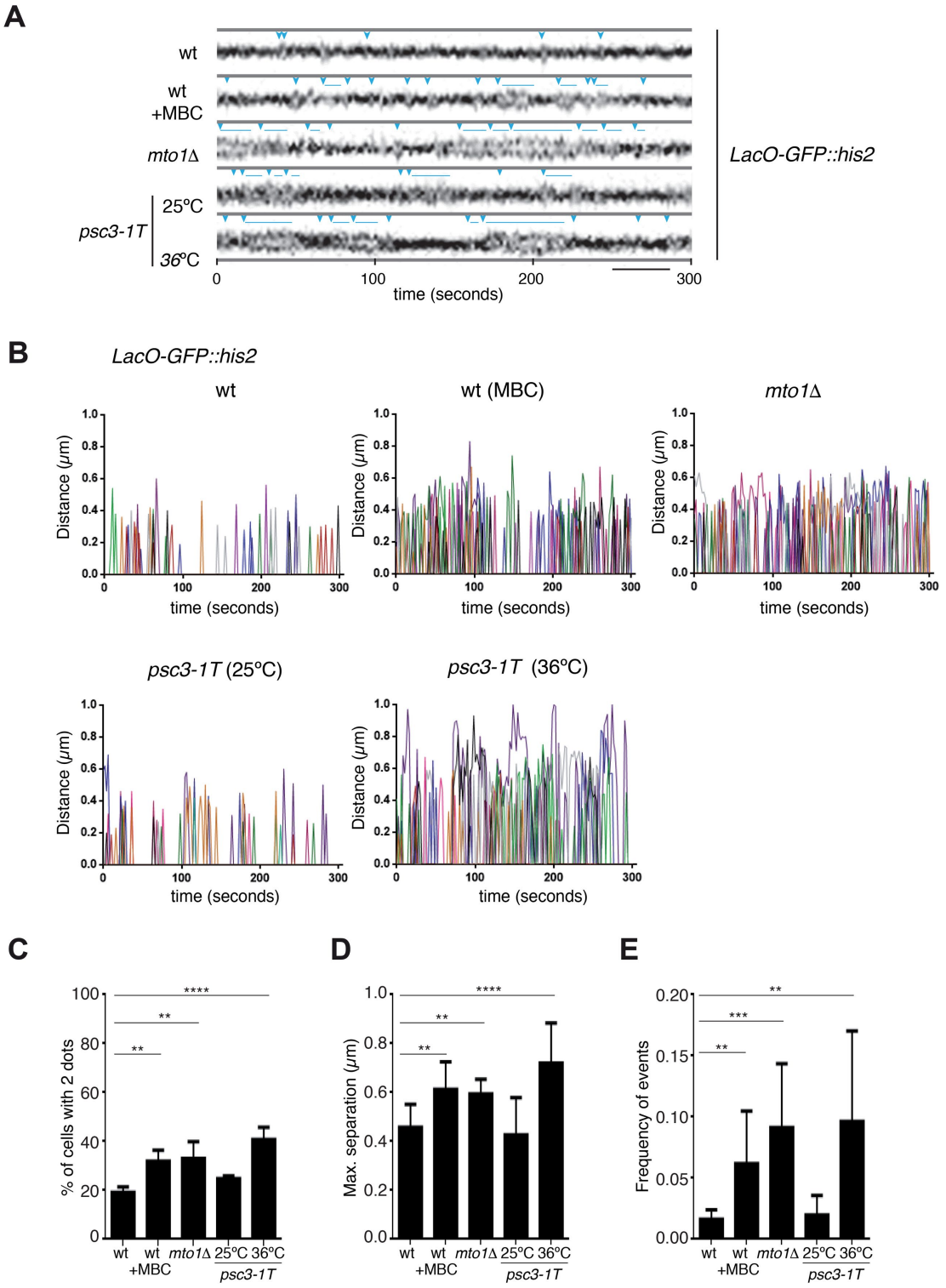


FIGURE 5: Defects in sister chromatid cohesion in *mto1Δ* and microtubule depolymerized cells. (A) Kymographs of representative examples of increased separation between sister chromatids as shown by GFP at *his2* locus in the indicated strains and conditions (blue arrowheads). Images are maximal projections of six *z*-sections with a step size of 0.4 μm acquired every 2 s. Scale bar: 2.5 μm. (B) Plots showing dynamics of loci in time-lapse images in the indicated strains and conditions. Distances between *his2* loci on sister chromatids are plotted over 300 s. Each color represents an individual cell ($n = 10$ cells). (C) Percentage of cells of the indicated strains and conditions showing separated GFP dots on *his2* loci at a single time point ($n = 50$ cells for each condition). *psc3-1T* cells were imaged at 25°C or after 2.5 h at 36°C. Error bars represent the SD from three independent experiments. (D) Graph showing the average maximum GFP-his2 loci separation observed over 300 s in cells shown in B. Error bars represent the SD. (E) Graph showing frequency of separation events per second in cells showed in B. Error bars represent the SD. **, $p < 0.01$; ***, $p < 0.001$; ****, $p < 0.0001$. wt, wild type.

MBC (Figure 5, A–C, and Supplemental Movies S1 and S2). In wild-type cells, loci showed on average 4.8 ± 2.3 separation events over a period of 5 min (Figure 5, A, B, and E, and Supplemental Figure S5). In cells treated with MBC and in *mto1*Δ cells, we observed an average of 18.4 ± 12.8 events and 27.2 ± 15.7 events, respectively, during the same time period (Figure 5, A, B, and E, and Supplemental Figure S5). The maximum distance reached between the loci was also increased in wild-type cells treated with MBC and in *mto1*Δ cells (0.61 ± 0.11 and 0.59 ± 0.05, respectively) compared with wild-type untreated cells (0.45 ± 0.09) (Figure 5, A, B, and D, and Supplemental Figure S5). The time that the loci spent apart was also increased. In wild-type cells, sister loci spent on average 2.2 ± 0.25 s apart, whereas in cells treated with MBC and *mto1*Δ cells, the loci spent on average 3.1 ± 1.1 and 4.6 ± 1.9 s apart, respectively, although we occasionally observed breathing events that persisted for >25 s (Figure 5, A and B, and Supplemental Figure S5).

We tested whether this breathing behavior is due to decreased cohesion between sister chromatids. To test this, we compared this behavior with that of a cohesin subunit mutant *psc3-1T* (Nonaka *et al.*, 2002). Cohesin mutants have been shown to exhibit a higher percentage of cells with sister chromatid or centromere separation in fixed samples (Tomonaga *et al.*, 2000; Bernard *et al.*, 2001; Tanaka *et al.*, 2001; Nonaka *et al.*, 2002), but the dynamics of chromosomal movements using live-cell imaging has not been previously shown. In time-lapse imaging of the *his2* loci, we found increased sister chromatid breathing in the temperature-sensitive *psc3-1T* mutant at nonpermissive temperature (Figure 5, A–E). These behaviors were similar but slightly more severe than those seen in the *mto1* mutant. Thus, the *mto1* mutant and cells treated with MBC exhibit defects similar to those of the *psc3* cohesin mutant.

We also assayed breathing behavior of chromosomal arrays at the *lys1* site, close to the centromere (Supplemental Figures S4, A–E, and S6). Here, we also detected similar breathing events. However, in contrast to the *his2* site, the frequency of these events at *lys1* was significantly elevated in the *psc3-1T* mutant, but not in *mto1*Δ and MBC-treated cells. This suggests that cohesion at the centromere is defective in the *psc3-1T* mutant but not in the *mto1*Δ mutant.

This defect in sister chromatid cohesion raises the possibility that Mto1 and microtubules affect the distribution or function of the cohesin complex. We used cohesin subunit Rad21 as a marker for the cohesin complex (Tomonaga *et al.*, 2000). Rad21-GFP protein localizes at the nuclear periphery to cohesin-enriched loci such as centromeres, telomeres, and rDNA (Tomonaga *et al.*, 2000; Tanaka *et al.*, 2001; Nakazawa *et al.*, 2015; Reyes *et al.*, 2015). Rad21-GFP localization was similar in wild-type, *mto1*Δ, and MBC-treated cells (Figure 6A and Supplemental Figure S7), suggesting that cohesin is still present at these sites. Western blots showed that the total protein levels of Rad21-9Pk are similar in *mto1*Δ and wild-type cells (Figure 6B).

We next tested for Rad21 binding at chromosomal sites by chromatin immunoprecipitation (ChIP). We sampled binding at five loci that have been previously shown to have different levels of cohesin loaded in normal conditions (Figure 6C) (Schmidt *et al.*, 2009): The centromeric dh repeat locus represent cohesin-rich sites. Additional cohesin-associated regions include positions Chr II 2.13 Mb (site d), which is 10 kb apart from the *his2* locus, Chr II 1.25 Mb (site a), and Chr II 1.26 Mb (site b). Chr II 0.178 Mb (site c) is a cohesin-poor position. At four of the five chromosomal sites, we found a significant decrease (>50%) in cohesin binding in *mto1*Δ compared with wild type (Figure 6C). However, at centromeric dh repeats, we found no detectable difference in Rad21 binding between wild-type and *mto1*Δ cells. Similar results were seen in three independent experiments. Thus, *mto1*Δ cells exhibit a defect in Rad21 cohesin binding at chromosomal loci on chromosomal arms but retain normal Rad21 binding at centromeres. These results are consistent with live-cell imaging results showing increased sister chromatid breathing at the *his2* locus (near site d), but not the *lys1* locus (near the centromere) (Figure 5 and Supplemental Figures S4–S6).

In summary, these results show that *mto1*Δ cells have a defect in sister chromatid cohesion that is likely due to abnormal cohesin distribution along chromosomal arms. It is well established that cohesion defects result in defects in DNA repair (Birkenbihl and Subramani, 1992; Sjogren and Nasmyth, 2001; Wu and Yu, 2012), and thus, this cohesin defect provides an explanation for the DNA repair and HR defects in *mto1*Δ cells.

## DISCUSSION

In this study, we show that the MT nucleation factor Mto1 is needed for efficient DNA repair, HR, and sister chromatid cohesion at chromosomal arms in interphase fission yeast cells. We find that *mto1*Δ mutants have defects in cohesin binding and sister chromatid pairing (Figures 5 and 6), which explain at least in part the defects in DNA repair and HR (Figures 3 and 4). We also show that transient inhibition of cytoplasmic MTs by treating interphase cells with MBC produces similar phenotypes in DNA repair factories and sister chromatid pairing (Figure 3 and 5). As Mto1 and MTs are outside the nucleus during interphase, these data lead to an intriguing model that the attachment of cytoplasmic MTs to the nucleus is needed for chromosomal functions such as cohesion and DNA repair. The results presented here provide the initial demonstration of a role for MTs and Mto1 in sister chromatin pairing and cohesin loading or distribution onto chromosomal arms.

How might cytoplasmic MTs and Mto1 affect chromosomal processes? The cytoplasmic MT bundles are physically attached to chromosomes through the NE, the SPB, and other sites containing SUN-KASH complexes (Hagan and Yanagida, 1995; Ding *et al.*, 2004; Chikashige *et al.*, 2006; Hou *et al.*, 2012; Fernandez-Alvarez *et al.*, 2016; Bao *et al.*, 2018). Pushing forces of these MT bundles at the cell tips produce oscillatory movements of the SPB and the chromosomes inside the nucleus (Daga *et al.*, 2006; Daga and Nurse, 2008; Swartz *et al.*, 2014; Schreiner *et al.*, 2015). We show that these chromosomal movements, which affect centromeric chromatin and chromosomal arms, are dependent on MTs and Mto1 (Figure 1). One attractive model is that these MT-dependent forces might facilitate cohesin loading or distribution early in the cell cycle (G1/S) and consequently affect the efficiency of DNA repair (discussed below). An alternate model is that MTs and Mto1 are needed for proper organization or functioning of NE complexes with roles in general chromosomal organization (Swartz *et al.*, 2014). In a third model, Mto1 and perhaps postmitotic MTs function directly at the chromosome inside the nucleus. In mammalian cells, for instance, γ-tubulin has been found in complex with Rad51 in the nucleus in response to genotoxic treatments (Lesca *et al.*, 2005; Oakley *et al.*, 2015). However, we did not detect Mto1 inside the nucleus and it does not appear to colocalize with DNA repair factories (Supplemental Figure S2), although our experiments could not rule out, for instance, whether Mto1 associates with the nuclear face of the SPB.

Chromosomal movements driven by the cytoskeleton are likely to play diverse functions in nuclear processes, including dynamic chromosomal organization, homology searching and pairing, detangling of chromosomes, and stimulation of mechanosensitive processes. In meiosis, cytoskeleton-based forces from actin or MTs facilitate recombination and synaptonemal complex formation in fission yeast (Ding *et al.*, 2004), budding yeast (Conrad *et al.*, 2008; Koszul *et al.*, 2008), and *C. elegans* (Sato *et al.*, 2009). There are a

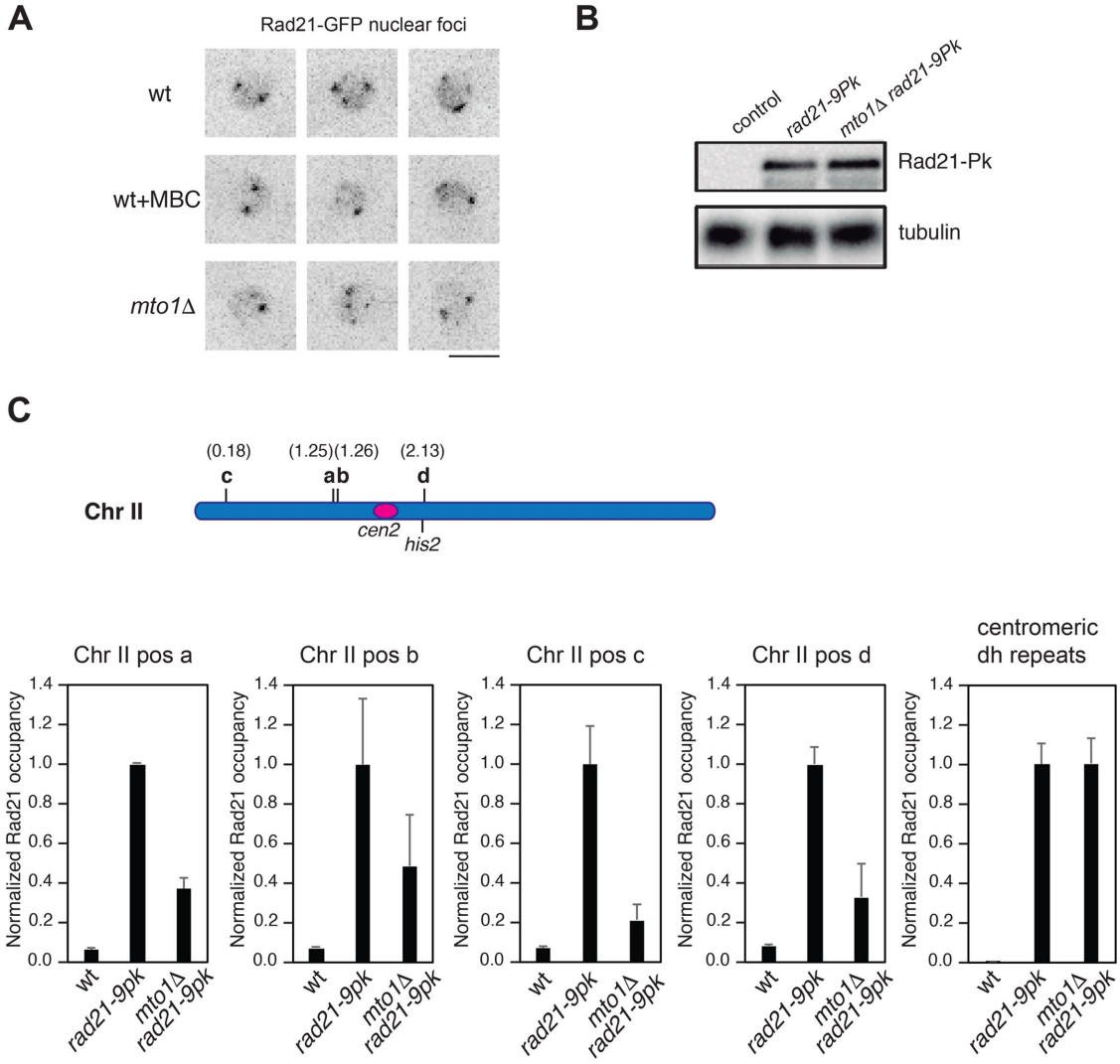


**FIGURE 6:** Defects in chromatin-bound cohesin in *mto1*Δ cells. (A) Overall nuclear organization of cohesin subunit Rad21-GFP is similar in wild-type (wt), MBC-treated, and *mto1*Δ cells. Images are maximal projections of representative nuclei. (B) Western blots showing equivalent levels of Rad21-9Pk in wild-type and *mto1*Δ strains probed with anti-Pk antibody, with tubulin shown as loading control. (C) Schematic map of chr II indicating the centromere, the *his2* locus, and positions a–d probed for Rad21 binding. ChIP of Rad21-9Pk in the indicated strains followed by qPCR assaying centromeric dh repeats and four chromosomal sites on Chr II arms (sites a to d; see *Materials and Methods* for genomic positions). Error bars represent the SD from three independent experiments ($p < 0.001$).

number of differences, however, between mitotic and meiotic processes. The magnitude of nuclear oscillation during interphase is much smaller compared with meiotic horsetail movement, during which the nucleus rapidly moves between the two ends of the cell (Chikashige *et al.*, 1994; Sjogren and Nasmyth, 2001; Chacón *et al.*, 2016). In addition, meiotic movements are driven by force application to telomeres, while interphase movements are primarily transmitted to centromeres and have less effect on distal chromosomal areas (Chikashige *et al.*, 1994; Swartz *et al.*, 2014). Moreover, the precise nature and molecular control of HR events are quite different between HR in homologous chromosomes in meiosis and in the mitotic cell cycle, wherein the main source of an HR donor sequence for DNA repair is the sister chromatid linked by cohesin complexes to the damaged DNA sequence. Chromosomal movements may also contribute to DNA repair and recombination processes. Microtubules may directly or indirectly contribute to the increased mobility of chromosomal loci observed in response to DNA damage in budding and fission yeast (Dion *et al.*, 2012; Mine-Hattab and Rothstein, 2012; Swartz *et al.*, 2014; Lawrimore *et al.*, 2017). In budding yeast, microtubules are needed for the DNA damage induction of telomere mobilization that contributes to increased mobility of the genome (Lawrimore *et al.*, 2017). While our work was in revision, a report appeared showing that, in budding yeast, abnormally strong MT forces may cause increased DNA repair defects through effects of compressive forces on the nucleus as it migrates through the small bud neck (Estrem and Moore, 2019); as fission yeast nuclei do not encounter a similar bud neck constriction, it is unlikely that they experience these types of compression forces.

Our findings elucidate a new function for the cytoskeleton in DNA repair and recombination: Mto1 and MTs are needed for sister chromatid cohesion. In the absence of Mto1 or the cohesin subunit Psc3, sister loci undergo transient, frequent breathing events in which chromosomal loci move apart and then come back together (Figure 5). Cohesins are loaded at centromeres and other sites by

| Strain origin | Strain no. | Genotype |
|---|---|---|
| This study | 2452 | *h90 sid2-tdTomato::NatR lys1::LacOp his7+::LacI-GFP-NLS* |
| This study | 2822 | *h90 mto1Δ::kanMX6 sid2-tdTomato::natMX6 lys1::LacOp his7+::LacI-GFP-NLS* |
| Chang lab collection | 1845 | *h- mto1Δ::kanMX6 ura4-D18 leu1-32* |
| Daga lab collection | 2020 | *h+ rad3Δ::ura4+ ura4-D18 leu1-32* |
| This study | 2022 | *h- rad3Δ::ura4+ mto1Δ::kanMX6 ura4-D18 leu1-32* |
| Daga lab collection | 1994 | *h- chk1Δ::ura4+ ura4-D18 leu1-32* |
| This study | 1866 | *h- mto1Δ::kanMX6 chk1Δ::ura4+ ura4-D18 leu1-32* |
| Daga lab collection | 2034 | *h cds1Δ::ura4+ ura4-D18 leu1-32* |
| This study | 2037 | *h cds1Δ::ura4+ mto1Δ::kanMX6 ura4-D18 leu1-32* |
| Sawin lab | KS2010 | *h+ mto1-9A2 ade6-M216 leu1-32 ura4-D18* |
| Sawin lab | KS1957 | *h- mto1(1-1051):ura4+ ade6-M210 leu1-32* |
| Sawin lab | KS1957 | *h+ mto2Δ::kanMX6 ade6-M216 leu1-32 ura4-D18* |
| Daga lab collection | 1805 | *h+ tip1Δ::kanMX leu1-32ade6-* |
| Jia lab | 2686 | *h+ csi1Δ::natMX6 ade6-leu1-32ura4-D18* |
| Hiraoka lab | 2691 | *h+ his2 ade6-M216 leu1 ura4-D18 lys1 ima1Δ::hphNT1* |
| Hiraoka lab | 2693 | *h+ his2 ade6-M216 leu1 ura4-D18 lys1 ish-GFP:kanMX6 man1Δ::LEU2+* |
| Hiraoka lab | 2694 | *h+ his2 ade6-M216 leu1 ura4-D18 lys1 ish-GFP:kanMX6 lem2Δ::ura4+* |
| Hiraoka lab | 2695 | *h+ his2 ade6-M216 leu1 ura4-D18 lys1 ish-GFP:kanMX6 ima1Δ::hphNT1 lem2Δ::ura4* |
| Meister lab | 1803 | *h+ rad52-YFP::kanMX6 leu1-32ura4-D18* |
| This study | 1785 | *h- rad52-YFP::kanMX6 mto1Δ::kanMX6 ura4-D18 leu1-32* |
| This study | 2712 | *h mto2Δ::kanMX6 rad52-YFP::kanMX6 ura4-D18 leu1-32* |
| This study | 2340 | *h90 sid2-tdTomato::natMX6 his2[::kanMX6-ura4+ LacOp]his7+::lacI-GFP leu1-32 ade6- leu1-32* |
| This study | 2341 | *h90 mto1Δ::kanMX6 sid2-tdTomato::natMX6his2::kanMX6-ura4+ LacOp his7+::lacI-GFP leu1-32 ade6- leu1-* |
| This study | 7700 | *h psc3-1T-kanMX6 his2::kanMX6-ura4+ LacOp his7+::lac Sid2:tomato:NatMX leu1-32 GFP ade6-leu1-32 his-* |
| This study | 7701 | *h psc3-1T-kanMX6 lys1::kanMX6-ura4+ LacOp his7+::lac Sid2:tomato:NatMX leu1-32 GFP ade6-leu1-32 his-* |
| TH805 | 2203 | *h ade6-M210 leu1-32 ura4-D18 Ch16-MG* |
| This study | 2206 | *h mto1Δ::natR ade6-M210 leu1-32 ura4-D18 Ch16-MG* |
| TH844 | 2250 | *h ade6-M210 leu1-32 ura4-D18 Ch16-MG pREP81X-HO* |
| This study | 2253 | *h+ mto1Δ::natR ade6-M210 leu1-32 ura4-D18 Ch16-MG pREP81X-HO* |
| TH877 | 2272 | *h rad3Δ::ura4+ ade6-M210 leu1-32 ura4-D18 Ch16-MG pREP81X-HO* |
| This study | 2287 | *h rad3Δ::ura4+ ade6-M210 leu1-32 ura4-D18 Ch16-MG* |
| This study | 2397 | *h mto1Δ::natR rad3Δ::ura4+ ade6-M210 L- U- Ch16-MG pREP81X-HO* |
| This study | 2399 | *h mto1Δ::natR rad3Δ::ura4+ ade6-M210 L- U- Ch16-MG* |
| MCW1262 | 2814 | *h- ura4-D18 leu1-32 his3-D1 arg3-D4 ade6-M375 int::pUC8/his3+/RTS1 siteA orientation1/ade6-L469* |
| This study | 3662 | *h- mto1Δ ura4-D18 leu1-32 his3-D1 arg3-D4 ade6-M375 int::pUC8/his3+/RTS1 siteA orientation1/ade6-L469* |
| MCW1362 | 2816 | *h- swi1Δ ura4-D18 leu1-32 his3-D1 arg3-D4 ade6-M375 int::pUC8/his3+/RTS1 siteA orientation1/ade6-L469* |
| This study | 3666 | *h- mto1Δ swi1Δ ura4-D18 leu1-32 his3-D1 arg3-D4 ade6-M375 int::pUC8/his3+/RTS1 siteA orientation1/ade6-L469* |
| MCW1433 | 2815 | *h- ura4-D18 leu1-32 his3-D1 arg3-D4 ade6-M375 int::pUC8/his3+/RTS1 siteA orientation2/ade6-L469* |

**TABLE 1:** Strains used in this study.

Continues

| Strain origin | Strain no. | Genotype |
|---|---|---|
| This study | 3664 | *h- mto1Δ ura4-D18 leu1-32 his3-D1 arg3-D4 ade6-M375 int::pUC8/his3+/RTS1 siteA orientation2/ade6-L469* |
| MCW1358 | 2817 | *h- swi1Δ ura4-D18 leu1-32 his3-D1 arg3-D4 ade6-M375 int::pUC8/his3+/RTS1 siteA orientation2/ade6-L469* |
| This study | 3668 | *h- mto1Δ swi1Δ ura4-D18 leu1-32 his3-D1 arg3-D4 ade6-M375 int::pUC8/his3+/RTS1 siteA orientation2/ade6-L469* |
| This study | 2867 | *h- mto1Δ::natMX6 rad21-9PK:kanMX6 leu1-32* |
| This study | 2870 | *h mto1Δ::kanMX6 rad21-3EGFP:kanMX6 leu1-32* |
| JP3789 | 2850 | *h- rad21-9PK:kanMX6* |
| This study | 4585 | *h cnp1-mCherry-KanMX rad21-3GFP-KanMX6 ura4-D18 leu1-32 ade6-M375* |
| This study | 4675 | *h cnp1-mCherry-KanMX rad21-3GFP-KanMX6 mto1Δ::kanMX ura4-D18 leu1-32 ade6-M375* |
| This study | 7702 | *h mto1-mCherry-Nat rad52-YFP::kanMX6* |
| This study | 6727 | *h mto1-mCherry-Nat cut11-GFP:ura4+* |

**TABLE 1:** Strains used in this study. Continued

cohesin-loading complexes before DNA replication and may spread laterally along chromosomes to sites of convergent transcription (Tanaka *et al.*, 2001; Lengronne *et al.*, 2004; Schmidt *et al.*, 2009; Peters and Nishiyama, 2012). Cohesin is also recruited during postreplication to sites of double-stranded breaks (Strom *et al.*, 2004). In the *mto1* mutant, we found defects in sister chromatid cohesion and a significant reduction of Rad21 cohesin at several cohesin associated sites, even in the absence of DNA damage (Figure 6). This defect may be a consequence of defective cohesin loading, maintenance, or distribution. We speculate that cohesin loading or its dynamic distribution may be a mechanosensitive process dependent on MT-based forces. Specifically, the oscillatory movements of the SPB linked to centromeres provide tension on the pericentric regions of the chromosomes that could be necessary for efficient cohesin spreading. Whether cohesin defects may account for other cytoskeletal effects on chromosomal processes remains to be tested. Future studies may focus on how mechanical forces regulate cohesin dynamics and function. In general, understanding how chromosomal processes sense and respond to mechanical forces promises to reveal new dimensions in chromosomal biology.

## MATERIALS AND METHODS

### Strains and media

Strains used in this study are listed in Table 1. Standard fission yeast techniques and growth media were used (Moreno *et al.*, 1991). Cells were grown in YES media at 25 or 30°C, as indicated. Strains were prepared by crossing and (in the case of the HR assays) by genomic integration.

### Microscopy

A spinning-disk confocal microscope (Olympus IX81; Roper Scientific) was used. Cells were imaged using 461- and 562-nm lasers. Unless otherwise stated, *z*-stacks of 10 images with a *z*-step of 0.4 µm were collected using the 100× objective (UPlanSAPO, NA 1.4), and maximum projections were used for signal quantification. MetaMorph and ImageJ were used for image acquisition and analysis.

### Quantification of Rad52 intensity and dynamics

To follow Rad52-YFP factory dynamics, we acquired time-lapse images with a time interval of 2 min. We quantified peak nuclear signal of Rad52 over time from maximum-projection images, after subtracting the nuclear background signal. Alternatively, we also quantified background-corrected the total Rad52-YFP signal after thresholding the images to only include the Rad52-YFP factories.

### Microtubule depolymerization

For depolymerization of MTs, cells were grown to mid–log phase and attached to lectin-coated glass-bottom plates, and freshly prepared 10 µg/ml MBC was added to the cells. Late anaphase cells were marked and either directly imaged for 5–6 h to follow Rad52-GFP dynamics or tracked for 40–110 min and then imaged for 5 min to visualize Rad52 dynamics (Figure 3) or *his2* and *lys1* LacI-GFP dot "breathing" (Figure 5).

### Generation of DNA damage by laser

A single 10-ms pulse using an iLas system (Roper Scientific) with a 355-nm laser was targeted at a fixed area of 500 nm of the nuclei. The Rad52-YFP signal was subsequently followed by time-lapse imaging for an additional 25 min.

### Western blotting

To detect Pk-tagged Rad21, we used anti-Pk monoclonal antibody (kindly provided by I. Hagan, Cancer Research UK, Manchester Institute). Anti-tubulin antibody TAT-1 (kindly provided by Keith Gull, University of Oxford) was used to detect α-tubulin.

### Chromatin immunoprecipitation and real-time PCR

Strains expressing Rad21-9Pk–tagged protein at endogenous levels were fixed with 1% formaldehyde for 20 min, and chromatin was prepared according to Shan *et al.* (2016). Anti-Pk monoclonal antibody was used for immunoprecipitation, and primers targeting various several genomic regions were used for subsequent real-time PCR amplification of Rad21-bound DNA. Primer sequences (Table 2) correspond to positions 2.13, 0.178, 1.26, and 1.25 Mb on Chr II according to Schmidt *et al.* (2009). Real-time PCR signals were normalized to wild-type signal.

### Recombination assays

For HR detection, strains containing *mto1* deletion were prepared by crossing (in the case of the Chr16-MG–based system) and by homologous integration (for the intrachromosomal HR substrate). At least five independent clones of each genotype were tested to

| | |
|---|---|
| A forward | AATTGCAATCCTGAAGCTGGC |
| A reverse | CTTCAGCTAAATCCGTCATGC |
| B forward | CATGGATGCAGGTTGGTACG |
| B reverse | GCCTGGCGTAATAACAGCTT |
| C forward | AGAAGTTCAGCTCTCGGAAAA |
| C reverse | GTGTAATTTCCGTGAATCGTCA |
| D forward | GGAAACGGTTCGGGTATTCT |
| D reverse | TGACGCAGCTACTTCAATGG |

**TABLE 2:** Primer sequences used for real-time PCR of Rad21-Pk9 ChIP.

determine recombination frequency. In the RFB system, strains were streaked to single colonies on YES medium, then replica plated on selective ade$^-$ media, and individual *ade*$^-$ colonies were inoculated into liquid cultures and grown for 8 h at 30°C before plating. Cells were counted and plated in parallel on YES plates to determine total viable cell numbers and on plates lacking adenine to determine the number of adenine prototrophs generated by recombination. The numbers of cells plated were calculated to result in 100–200 growing colonies per plate. Colonies were counted after 3 d at 30°C, and recombination frequency was calculated as in Ahn *et al.* (2005). At least 300 adenine prototrophs from three biological repeats were counted for each condition.

For quantification of HR with the Chr16-MG substrate (Prudden *et al.*, 2003), cells were grown on ade$^-$, leu$^-$ plates containing thiamine and then transferred into liquid Edinburgh minimal media (EMM) lacking leucine for 16 h to induce HO endonuclease expression before plating. G418-resistant cells were replica plated on ade$^-$ plates to determine adenine prototrophy. Before calculating recombination frequency (Prudden *et al.*, 2003), we subtracted background rates of Chr16 loss unrelated to HR, which was calculated by plating uninduced cells on YES and then replica plating them on ade$^-$ plates.

## ACKNOWLEDGMENTS

We thank the Daga lab members and our colleagues at the Centro Andaluz de Biologia del Desarrollo for helpful discussions. We are grateful to Victor Carranco for excellent technical help and to Tatiana Garcia-Muse and Andrés Aguilera at the CABIMER, Seville, for the support in using the γ-ray irradiator. We also thank Iain Hagan, Yasushi Hiraoka, Tim Humphrey, Ken Sawin, and Matthew Whitby for kindly providing us with strains and reagents. We also thank Lorraine S. Symington for support in early work at Columbia University. This work was supported by grants from the Spanish Ministry of Economy and Competitiveness BFU2011-15216-E, P09-CTS-4697, and PGC2018-099849-B-100 to R.R.D.; National Institutes of Health (NIH) R01, GM067690, and GM115185 to F.C.; and NIH grants R01-GM085145 and R35-GM126910 to S.J.

## REFERENCES

Ahn JS, Osman F, Whitby MC (2005). Replication fork blockage by RTS1 at an ectopic site promotes recombination in fission yeast. EMBO J 24, 2011–2023.

Bao XX, Spanos C, Kojidani T, Lynch EM, Rappsilber J, Hiraoka Y, Haraguchi T, Sawin KE (2018). Exportin Crm1 is repurposed as a docking protein to generate microtubule organizing centers at the nuclear pore. eLife 7, e33465.

Barrales RR, Forn M, Georgescu PR, Sarkadi Z, Braun S (2016). Control of heterochromatin localization and silencing by the nuclear membrane protein Lem2. Genes Dev 30, 133–148.

Bernard P, Maure JF, Partridge JF, Genier S, Javerzat JP, Allshire RC (2001). Requirement of heterochromatin for cohesion at centromeres. Science 294, 2539–2542.

Birkenbihl RP, Subramani S (1992). Cloning and characterization of rad21 an essential gene of *Schizosaccharomyces pombe* involved in DNA double-strand-break repair. Nucleic Acids Res 20, 6605–6611.

Chacón MR, Delivani P, Tolić IM (2016). Meiotic nuclear oscillations are necessary to avoid excessive chromosome associations. Cell Rep 17, 1632–1645.

Chikashige Y, Ding DQ, Funabiki H, Haraguchi T, Mashiko S, Yanagida M, Hiraoka Y (1994). Telomere-led premeiotic chromosome movement in fission yeast. Science 264, 270–273.

Chikashige Y, Tsutsumi C, Yamane M, Okamasa K, Haraguchi T, Hiraoka Y (2006). Meiotic proteins bqt1 and bqt2 tether telomeres to form the bouquet arrangement of chromosomes. Cell 125, 59–69.

Christophorou N, Rubin T, Bonnet I, Piolot T, Arnaud M, Huynh JR (2015). Microtubule-driven nuclear rotations promote meiotic chromosome dynamics. Nat Cell Biol 17, 1388–1400.

Conrad MN, Lee CY, Chao G, Shinohara M, Kosaka H, Shinohara A, Conchello JA, Dresser ME (2008). Rapid telomere movement in meiotic prophase is promoted by NDJ1, MPS3, and CSM4 and is modulated by recombination. Cell 133, 1175–1187.

Crisp M, Liu Q, Roux K, Rattner JB, Shanahan C, Burke B, Stahl PD, Hodzic D (2006). Coupling of the nucleus and cytoplasm: role of the LINC complex. J Cell Biol 172, 41–53.

Daga RR, Nurse P (2008). Interphase microtubule bundles use global cell shape to guide spindle alignment in fission yeast. J Cell Sci 121, 1973–1980.

Daga RR, Yonetani A, Chang F (2006). Asymmetric microtubule pushing forces in nuclear centering. Curr Biol 16, 1544–1550.

Ding DQ, Yamamoto A, Haraguchi T, Hiraoka Y (2004). Dynamics of homologous chromosome pairing during meiotic prophase in fission yeast. Dev Cell 6, 329–341.

Dion V, Kalck V, Horigome C, Towbin BD, Gasser SM (2012). Increased mobility of double-strand breaks requires Mec1, Rad9 and the homologous recombination machinery. Nat Cell Biol 14, 502–509.

Estrem C, Moore JK (2019). Astral microtubule forces alter nuclear organization and inhibit DNA repair in budding yeast. Mol Biol Cell 30, 2000–2013.

Fabre E, Zimmer C (2018). From dynamic chromatin architecture to DNA damage repair and back. Nucleus 9, 161–170.

Fernandez-Alvarez A, Bez C, O'Toole ET, Morphew M, Cooper JP (2016). Mitotic nuclear envelope breakdown and spindle nucleation are controlled by interphase contacts between centromeres and the nuclear envelope. Dev Cell 39, 544–559.

Gonzalez Y, Saito A, Sazer S (2012). Fission yeast Lem2 and Man1 perform fundamental functions of the animal cell nuclear lamina. Nucleus 3, 60–76.

Hagan I, Yanagida M (1995). The product of the spindle formation gene sad1+ associates with the fission yeast spindle pole body and is essential for viability. J Cell Biol 129, 1033–1047.

Hampoelz B, Azou-Gros Y, Fabre R, Markova O, Puech PH, Lecuit T (2011). Microtubule-induced nuclear envelope fluctuations control chromatin dynamics in *Drosophila* embryos. Development 138, 3377–3386.

Harper L, Golubovskaya I, Cande WZ (2004). A bouquet of chromosomes. J Cell Sci 117, 4025–4032.

Harrison JC, Haber JE (2006). Surviving the breakup: the DNA damage checkpoint. Annu Rev Genet 40, 209–235.

Hartsuiker E, Vaessen E, Carr AM, Kohli J (2001). Fission yeast Rad50 stimulates sister chromatid recombination and links cohesion with repair. EMBO J 20, 6660–6671.

Herbert KM, Greenleaf WJ, Block SM (2008). Single-molecule studies of RNA polymerase: motoring along. Annu Rev Biochem 77, 149–176.

Hiraoka Y, Maekawa H, Asakawa H, Chikashige Y, Kojidani T, Osakada H, Matsuda A, Haraguchi T (2011). Inner nuclear membrane protein Ima1 is dispensable for intranuclear positioning of centromeres. Genes Cells 16, 1000–1011.

Hoog JL, Antony C (2007). Whole-cell investigation of microtubule cytoskeleton architecture by electron tomography. Methods Cell Biol 79, 145–167.

Hou H, Zhou Z, Wang Y, Wang J, Kallgren SP, Kurchuk T, Miller EA, Chang F, Jia S (2012). Csi1 links centromeres to the nuclear envelope for centromere clustering. J Cell Biol 199, 735–744.

Jessberger R (2002). The many functions of SMC proteins in chromosome dynamics. Nat Rev Mol Cell Biol 3, 767–778.

Kim KD, Tanizawa H, Iwasaki O, Corcoran CJ, Capizzi JR, Hayden JE, Noma K (2013). Centromeric motion facilitates the mobility of interphase genomic regions in fission yeast. J Cell Sci 126, 5271–5283.
Koszul R, Kim KP, Prentiss M, Kleckner N, Kameoka S (2008). Meiotic chromosomes move by linkage to dynamic actin cables with transduction of force through the nuclear envelope. Cell 133, 1188–1201.
Lawrence KS, Tapley EC, Cruz VE, Li Q, Aung K, Hart KC, Schwartz TU, Starr DA, Engebrecht J (2016). LINC complexes promote homologous recombination in part through inhibition of nonhomologous end joining. J Cell Biol 215, 801–821.
Lawrimore J, Barry TM, Barry RM, York AC, Friedman B, Cook DM, Akialis K, Tyler J, Vasquez P, Yeh E, Bloom K (2017). Microtubule dynamics drive enhanced chromatin motion and mobilize telomeres in response to DNA damage. Mol Biol Cell 28, 1701–1711.
Lengronne A, Katou Y, Mori S, Yokobayashi S, Kelly GP, Itoh T, Watanabe Y, Shirahige K, Uhlmann F (2004). Cohesin relocation from sites of chromosomal loading to places of convergent transcription. Nature 430, 573–578.
Lesca C, Germanier M, Raynaud-Messina B, Pichereaux C, Etievant C, Emond S, Burlet-Schiltz O, Monsarrat B, Wright M, Defais M (2005). DNA damage induce gamma-tubulin-RAD51 nuclear complexes in mammalian cells. Oncogene 24, 5165–5172.
Lindsay HD, Griffiths DJ, Edwards RJ, Christensen PU, Murray JM, Osman F, Walworth N, Carr AM (1998). S-phase-specific activation of Cds1 kinase defines a subpathway of the checkpoint response in *Schizosaccharomyces pombe*. Genes Dev 12, 382–395.
Lisby M, Mortensen UH, Rothstein R (2003). Colocalization of multiple DNA double-strand breaks at a single Rad52 repair centre. Nat Cell Biol 5, 572–577.
Lottersberger F, Karssemeijer RA, Dimitrova N, de Lange T (2015). 53BP1 and the LINC complex promote microtubule-dependent DSB mobility and DNA repair. Cell 163, 880–893.
Malone CJ, Fixsen WD, Horvitz HR, Han M (1999). UNC-84 localizes to the nuclear envelope and is required for nuclear migration and anchoring during *C. elegans* development. Development 126, 3171–3181.
Malone CJ, Misner L, Le Bot N, Tsai MC, Campbell JM, Ahringer J, White JG (2003). The *C. elegans* hook protein, ZYG-12, mediates the essential attachment between the centrosome and nucleus. Cell 115, 825–836.
Matsuda A, Asakawa H, Haraguchi T, Hiraoka Y (2017). Spatial organization of the *Schizosaccharomyces pombe* genome within the nucleus. Yeast 34, 55–66.
McGee MD, Rillo R, Anderson AS, Starr DA (2006). UNC-83 IS a KASH protein required for nuclear migration and is recruited to the outer nuclear membrane by a physical interaction with the SUN protein UNC-84. Mol Biol Cell 17, 1790–1801.
Meister P, Poidevin M, Francesconi S, Tratner I, Zarzov P, Baldacci G (2003). Nuclear factories for signalling and repairing DNA double strand breaks in living fission yeast. Nucleic Acids Res 31, 5064–5073.
Meister P, Taddei A, Vernis L, Poidevin M, Gasser SM, Baldacci G (2005). Temporal separation of replication and recombination requires the intra-S checkpoint. J Cell Biol 168, 537–544.
Mekhail K, Moazed D (2010). The nuclear envelope in genome organization, expression and stability. Nat Rev Mol Cell Biol 11, 317–328.
Mine-Hattab J, Rothstein R (2012). Increased chromosome mobility facilitates homology search during recombination. Nat Cell Biol 14, 510–517.
Misteli T, Soutoglou E (2009). The emerging role of nuclear architecture in DNA repair and genome maintenance. Nat Rev Mol Cell Biol 10, 243–254.
Molnar M, Doll E, Yamamoto A, Hiraoka Y, Kohli J (2003). Linear element formation and their role in meiotic sister chromatid cohesion and chromosome pairing. J Cell Sci 116, 1719–1731.
Moreno S, Klar A, Nurse P (1991). Molecular genetic analysis of fission yeast *Schizosaccharomyces pombe*. Methods Enzymol 194, 795–823.
Nakazawa N, Sajiki K, Xu X, Villar-Briones A, Arakawa O, Yanagida M (2015). RNA pol II transcript abundance controls condensin accumulation at mitotically up-regulated and heat-shock-inducible genes in fission yeast. Genes Cells 20, 481–499.
Neumann FR, Dion V, Gehlen LR, Tsai-Pflugfelder M, Schmid R, Taddei A, Gasser SM (2012). Targeted INO80 enhances subnuclear chromatin movement and ectopic homologous recombination. Genes Dev 26, 369–383.
Nonaka N, Kitajima T, Yokobayashi S, Xiao G, Yamamoto M, Grewal SI, Watanabe Y (2002). Recruitment of cohesin to heterochromatic regions by Swi6/HP1 in fission yeast. Nat Cell Biol 4, 89–93.
Oakley BR, Paolillo V, Zheng Y (2015). γ-Tubulin complexes in microtubule nucleation and beyond. Mol Biol Cell 26, 2957–2962.
Oza P, Jaspersen SL, Miele A, Dekker J, Peterson CL (2009). Mechanisms that regulate localization of a DNA double-strand break to the nuclear periphery. Genes Dev 23, 912–927.
Peters JM, Nishiyama T (2012). Sister chromatid cohesion. Cold Spring Harb Perspect Biol 4, a011130.
Prudden J, Evans JS, Hussey SP, Deans B, O'Neill P, Thacker J, Humphrey T (2003). Pathway utilization in response to a site-specific DNA double-strand break in fission yeast. EMBO J 22, 1419–1430.
Razafsky D, Hodzic D (2009). Bringing KASH under the SUN: the many faces of nucleo-cytoskeletal connections. J Cell Biol 186, 461–472.
Reyes C, Serrurier C, Gauthier T, Gachet Y, Tournier S (2015). Aurora B prevents chromosome arm separation defects by promoting telomere dispersion and disjunction. J Cell Biol 208, 713–727.
Rhind N, Russell P (2000). Chk1 and Cds1: linchpins of the DNA damage and replication checkpoint pathways. J Cell Sci 113 (Pt 22), 3889–3896.
Ryu T, Spatola B, Delabaere L, Bowlin K, Hopp H, Kunitake R, Karpen GH, Chiolo I (2015). Heterochromatic breaks move to the nuclear periphery to continue recombinational repair. Nat Cell Biol 17, 1401–1411.
Samejima I, Lourenco PC, Snaith HA, Sawin KE (2005). Fission yeast mto2p regulates microtubule nucleation by the centrosomin-related protein mto1p. Mol Biol Cell 16, 3040–3051.
Samejima I, Miller VJ, Groocock LM, Sawin KE (2008). Two distinct regions of Mto1 are required for normal microtubule nucleation and efficient association with the gamma-tubulin complex in vivo. J Cell Sci 121, 3971–3980.
Sato A, Isaac B, Phillips CM, Rillo R, Carlton PM, Wynne DJ, Kasad RA, Dernburg AF (2009). Cytoskeletal forces span the nuclear envelope to coordinate meiotic chromosome pairing and synapsis. Cell 139, 907–919.
Sawin KE, Lourenco PC, Snaith HA (2004). Microtubule nucleation at non-spindle pole body microtubule-organizing centers requires fission yeast centrosomin-related protein mod20p. Curr Biol 14, 763–775.
Schmidt CK, Brookes N, Uhlmann F (2009). Conserved features of cohesin binding along fission yeast chromosomes. Genome Biol 10, R52.
Schneider R, Grosschedl R (2007). Dynamics and interplay of nuclear architecture, genome organization, and gene expression. Genes Dev 21, 3027–3043.
Schreiner SM, Koo PK, Zhao Y, Mochrie SG, King MC (2015). The tethering of chromatin to the nuclear envelope supports nuclear mechanics. Nat Commun 6, 7159.
Shan CM, Wang J, Xu K, Chen H, Yue JX, Andrews S, Moresco JJ, Yates JR, Nagy PL, Tong L, Jia S (2016). A histone H3K9M mutation traps histone methyltransferase Clr4 to prevent heterochromatin spreading. eLife 5, e17903.
Sjogren C, Nasmyth K (2001). Sister chromatid cohesion is required for postreplicative double-strand break repair in *Saccharomyces cerevisiae*. Curr Biol 11, 991–995.
Steglich B, Filion GJ, van Steensel B, Ekwall K (2012). The inner nuclear membrane proteins Man1 and Ima1 link to two different types of chromatin at the nuclear periphery in *S. pombe*. Nucleus 3, 77–87.
Strom L, Lindroos HB, Shirahige K, Sjogren C (2004). Postreplicative recruitment of cohesin to double-strand breaks is required for DNA repair. Mol Cell 16, 1003–1015.
Swartz RK, Rodriguez EC, King MC (2014). A role for nuclear envelope-bridging complexes in homology-directed repair. Mol Biol Cell 25, 2461–2471.
Tanaka K, Hao Z, Kai M, Okayama H (2001). Establishment and maintenance of sister chromatid cohesion in fission yeast by a unique mechanism. EMBO J 20, 5779–5790.
Tomonaga T, Nagao K, Kawasaki Y, Furuya K, Murakami A, Morishita J, Yuasa T, Sutani T, Kearsey SE, Uhlmann F, *et al*. (2000). Characterization of fission yeast cohesin: essential anaphase proteolysis of Rad21 phosphorylated in the S phase. Genes Dev 14, 2757–2770.
Tran PT, Marsh L, Doye V, Inoue S, Chang F (2001). A mechanism for nuclear positioning in fission yeast based on microtubule pushing. J Cell Biol 153, 397–411.
Uhler C, Shivashankar GV (2017). Regulation of genome organization and gene expression by nuclear mechanotransduction. Nat Rev Mol Cell Biol 18, 717–727.
Venkatram S, Jennings JL, Link A, Gould KL (2005). Mto2p, a novel fission yeast protein required for cytoplasmic microtubule organization and anchoring of the cytokinetic actin ring. Mol Biol Cell 16, 3052–3063.

Venkatram S, Tasto JJ, Feoktistova A, Jennings JL, Link AJ, Gould KL (2004). Identification and characterization of two novel proteins affecting fission yeast gamma-tubulin complex function. Mol Biol Cell 15, 2287–2301.
Wu N, Yu H (2012). The Smc complexes in DNA damage response. Cell Biosci 2, 5.
Xu YJ (2016). Inner nuclear membrane protein Lem2 facilitates Rad3-mediated checkpoint signaling under replication stress induced by nucleotide depletion in fission yeast. Cell Signal 28, 235–245.
Zhang X, Lei K, Yuan X, Wu X, Zhuang Y, Xu T, Xu R, Han M (2009). SUN1/2 and Syne/Nesprin-1/2 complexes connect centrosome to the nucleus during neurogenesis and neuronal migration in mice. Neuron 64, 173–187.
Zhang X, Xu R, Zhu B, Yang X, Ding X, Duan S, Xu T, Zhuang Y, Han M (2007). Syne-1 and Syne-2 play crucial roles in myonuclear anchorage and motor neuron innervation. Development 134, 901–908.
Zhang Y, Smith CL, Saha A, Grill SW, Mihardja S, Smith SB, Cairns BR, Peterson CL, Bustamante C (2006). DNA translocation and loop formation mechanism of chromatin remodeling by SWI/SNF and RSC. Mol Cell 24, 559–568.
Zhou K, Rolls MM, Hall DH, Malone CJ, Hanna-Rose W (2009). A ZYG-12-dynein interaction at the nuclear envelope defines cytoskeletal architecture in the *C. elegans* gonad. J Cell Biol 186, 229–241.
Zimmerman S, Chang F (2005). Effects of {gamma}-tubulin complex proteins on microtubule nucleation and catastrophe in fission yeast. Mol Biol Cell 16, 2719–2733.